Magic configurations in moiré superlattice of bilayer photonic crystals: Almost-perfect flatbands and unconventional localization

Dung Xuan Nguyen, Xavier Letartre, Emmanuel Drouard, Pierre Viktorovitch, H Chau Nguyen, Hai Son Nguyen

Letter

Magic configurations in moiré superlattice of bilayer photonic crystals: Almost-perfect flatbands and unconventional localization

Dung Xuan Nguyen [1,*] Xavier Letartre [2] Emmanuel Drouard [2] Pierre Viktorovitch,[2] H. Chau Nguyen,[3] and Hai Son Nguyen [2,4,†]

[1]*Brown Theoretical Physics Center and Department of Physics, Brown University, 182 Hope Street, Providence, Rhode Island 02912, USA*
[2]*Université de Lyon, École Centrale de Lyon, CNRS, INSA Lyon, Université Claude Bernard Lyon 1, CPE Lyon, CNRS, INL, UMR5270, 69130 Écully, France*
[3]*Naturwissenschaftlich-Technische Fakultät, Universität Siegen, Walter-Flex-Straße 3, 57068 Siegen, Germany*
[4]*Institut Universitaire de France (IUF), Paris, France*

(Received 9 May 2021; revised 20 May 2022; accepted 1 June 2022; published 19 August 2022)

We investigate the physics of photonic band structures of the moiré patterns that emerged when overlapping two unidimensional photonic crystal slabs with mismatched periods. The band structure of our system is a result of the interplay between intralayer and interlayer coupling mechanisms, which can be fine-tuned via the distance separating the two layers. We derive an effective Hamiltonian that captures the essential physics of the system and reproduces all numerical simulations of electromagnetic solutions with high accuracy. Most interestingly, *magic distances* corresponding to the emergence of photonic flatbands within the whole Brillouin zone of the moiré superlattice are observed. We demonstrate that these flatband modes are tightly localized within a moiré period. Moreover, we suggest a single-band tight-binding model that describes the moiré minibands, of which the tunneling rate can be continuously tuned via the interlayer strength. Our results show that the band structure of bilayer photonic moiré can be engineered in the same fashion as the electronic/excitonic counterparts. It would pave the way to study many-body physics at photonic moiré flatbands and optoelectronic devices.

DOI: 10.1103/PhysRevResearch.4.L032031

Moiré structures have been of central interest in fundamental physics during the last few years. The most important milestone is the discovery of flatbands in moiré patterns, which emerged when two graphene layers were overlapped at certain magic twisted angles [1–3], leading to nonconventional superconductivity [4–6] and strongly correlating insulator states with nontrivial topology [7,8]. Motivated by the electronic *magic angles*, photonic moiré has attracted tremendous research in light of shaping optical phenomena [9]. Hu *et al.* [10,11] have demonstrated the topological transition of photonic dispersion in twisted two-dimensional (2D) materials. However, the operating wavelength in these pioneering works are much larger than the moiré period; thus, dispersion engineering is based on the anisotropy of an effective medium rather than the microscopic moiré pattern. On the other hand, Wang *et al. [12]* have recently reported on the realization of a 2D photonic moiré superlattice. Nevertheless, their work only focused on light scattering through the moiré pattern, but the lattice is on the same plane, and there is no bilayer nor twisting concepts. Most recently, numerical [13] and tight-binding [14] methods have been proposed to investigate twisted bilayer photonic crystal slabs. It has been showed that local flatbands would be achieved [9,14] in twisted bilayer photonic crystal at small twisted angles. The photonic flatband also leads to the ultraslow photon [15]; the phenomenon was investigated in alternative systems [16,17].

In this letter, we report on a theoretical study of photonic band structures in moiré patterns that emerged when two mismatched one-dimensional (1D) subwavelength photonic crystal slabs were overlapped. The essential physics of the system can be captured by an effective four-component Hamiltonian. Accompanying the analytical theory, numerical electromagnetic simulations are performed with a case study of silicon structures operating at telecom wavelength. The obtained band structures result from an interplay between intralayer and interlayer coupling mechanisms which are tuned via the distance separating the two layers. Importantly, *magic distances* corresponding to the emergence of photonic flatbands within the whole Brillouin zone are demonstrated. The minibands of a moiré superlattice can be described by a single-band tight-binding model with Wannier functions tightly confined within a moiré period. The tunneling rate of light between nearest neighbor Wannier states is continuously modulated by the interlayer distance and vanished at magic distances, leading to flatband formation and photonic localization. Despite its simplicity, this 1D setup captures the interesting physics of moiré systems of twisted 2D materials. Our findings suggest that moiré photonics is a promising strategy to engineer photonic band structures for fundamental research and optoelectronic devices.

*dung_x_nguyen@brown.edu
†hai_son.nguyen@ec-lyon.fr

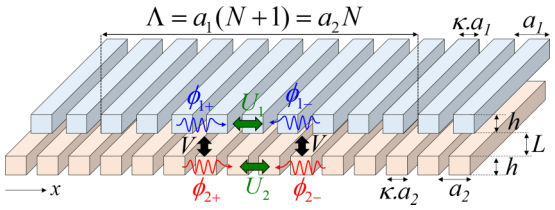

FIG. 1. Moiré superlattice of two gratings with periods a_1 and a_2 satisfying $a_1/a_2 = N/(N+1)$.

Our system consists of two 1D photonic crystal slabs which are two subwavelength high-refractive-index contrast gratings (Fig. 1). These gratings have the same subwavelength thickness h and filling fraction κ and are separated by only a subwavelength distance L. Their periods a_1 and a_2 are slightly different but satisfying the commensurate condition $a_1/a_2 = N/(N+1)$ for a natural number N [18]. The period of the superlattice is given by $\Lambda = (N+1)a_1 = Na_2$, consisting of $N+1$ periods of the upper grating and N periods of the lower one. In the regime of $N \gg 1$, a *semicontinuous approach* can be implemented: the two gratings are almost identical, and the moiré pattern corresponds to a continuous shifting function $\delta(x)$ of the upper grating with respect to the lower grating, given by $\delta(0 \leqslant x \leqslant \Lambda) = x/N$. The shifting δ sweeps an amount $a_0 = (a_1 + a_2)/2$ when x varies across a moiré period. In other words, the moiré superlattice is obtained from the bilayer lattice by introducing a slight period mismatch: the period of the upper grating is shrunken from a_0 to a_1, and the period of the lower one is stretched from a_0 to a_2. This configuration leads to a modulated relative displacement $\delta(x)$ with respect to the coordinate x. Two special configurations of $\delta/a_0 = 0$ and 0.5 are referred to as *AA* and *AB* stackings, resembling the terminology in bilayer graphene structures [19]. The moiré pattern is a period of a superlattice made of bilayer structures varying continuously from *AA* to *AB* stackings. The period mismatch leads to a Brillouin zone mismatch, and the size of the mini-Brillouin zone K_M is given by $K_M = K_1 - K_2$, where $K_1 = 2\pi/a_1$ and $K_2 = 2\pi/a_2$.

In our perturbation approach, the dispersion characteristic of the moiré superlattice is derived from two coupling mechanisms among forward (ϕ_{1+}, ϕ_{2+}) and backward (ϕ_{1-}, ϕ_{2-}) fundamental guided waves of the two noncorrugated slabs with effective refractive index: (i) Intralayer coupling due to the diffractive processes [20] between counterpropagating waves from the same layer and (ii) interlayer coupling via evanescence between copropagating waves from separated layers. Using $(\phi_{1+}, \phi_{1-}, \phi_{2+}, \phi_{2-})$ as a basis, eigenmodes of the system are described by the following Hamiltonian (detailed derivation is given in the Supplemental Material [21]):

$$H = \begin{bmatrix} -iv\partial_x + \omega_1 & U_1 & V & 0 \\ U_1 & iv\partial_x + \omega_1 & 0 & V \\ V & 0 & -iv\partial_x + \omega_2 & U_2\exp(-iK_M x) \\ 0 & V & U_2\exp(iK_M x) & iv\partial_x + \omega_2 \end{bmatrix}, \tag{1}$$

Here, $U_{1,2}$ are the intralayer coupling rates, V is the interlayer one, and v and $\omega_{1,2}$ are the group velocity and offset energy of the guided waves at the Brillouin zone edge for each grating, respectively. A slight difference of values of the offset pulsation and the intralayer coupling strength for each grating is due to the period mismatch, with $\omega_1 \approx \omega_2 \approx \omega_0$ and $U_1 \approx U_2 \approx U$, where ω_0 and U are the offset pulsation and the intralayer coupling strength in the grating of period a_0, respectively.

The energy-momentum dispersion is simulated numerically using the rigorous coupled-wave analysis (RCWA) method [22–24]. The numerical results corresponding to $N = 13$ when increasing the separation distance L are presented in Figs. 2(a)–2(e). When L is comparable with a_0, the band structure is simply the folding of single-layer dispersions [Fig. 2(a)]. It suggests that the interlayer coupling mechanism is negligible with respect to the intralayer ones (i.e., $V \ll U$) for $L \gtrsim a_0$. In this configuration, a bandgap, purely due to the intralayer coupling mechanism, is observed [Fig. 2(a)]. In analogy to semiconductor terminology, we refer to these upper/lower bands as *conductionlike*/*valencelike*. When $L \lesssim a_0$, the band hybridization due to the interlayer coupling results in the formation of a pair of particle-hole minibands, referred to as *electronlike*/*holelike* moiré bands [Figs. 2(b)–2(e)]. These two bands emerge within the bandgap of uncoupled layers and are well isolated from the conductionlike/valencelike continuum. In the following, we will pay particular attention to the behavior of these two bands when tuning the interlayer interaction. One may note that, with the choice of $a_0 = 300$ nm, the spectral range of the these band is in the telecom (i.e., $\sim$1.5 μm). Intriguingly, there are some specific values of L at which the bandwidth of these bands becomes almost zero, and these moiré bands are nearly perfectly flat. Figures 2(c) and 2(d) depict the band structures with a flat holelike moiré band and almost-flat electronlike band. Inspired by the analogy with the appearance of flatbands at magic angles in twisted bilayer graphene [2], we called these values magic distances. The moiré band structure is calculated using the Hamiltonian model given by Eq. (1), taking v, U, ω_0, and V as input parameters. These parameters are retrieved from the simulation of single and bilayer lattices [21,25]. Figures 2(f)–2(j) depict the band structures obtained by analytical calculations. These results quantitatively reproduce the numerical results presented in Figs. 2(a)–2(e), showing the emergence of moiré states within the bandgap and their flattening at magic distances. Noticeably, there is a slight difference between simulation and analytical results: the RCWA suggests that the flattening of the electronlike band always takes place at a slightly smaller distance L than the one of the holelike band, while the Hamiltonian model predicts that both bands become flat almost simultaneously.

The *global spectral bandwidth*, defined as $\Delta\omega = \max_q(\omega) - \min_q(\omega)$, is used as the figure of merit to evaluate the flatness of moiré minibands. Figures 3(a)–3(c) depict the

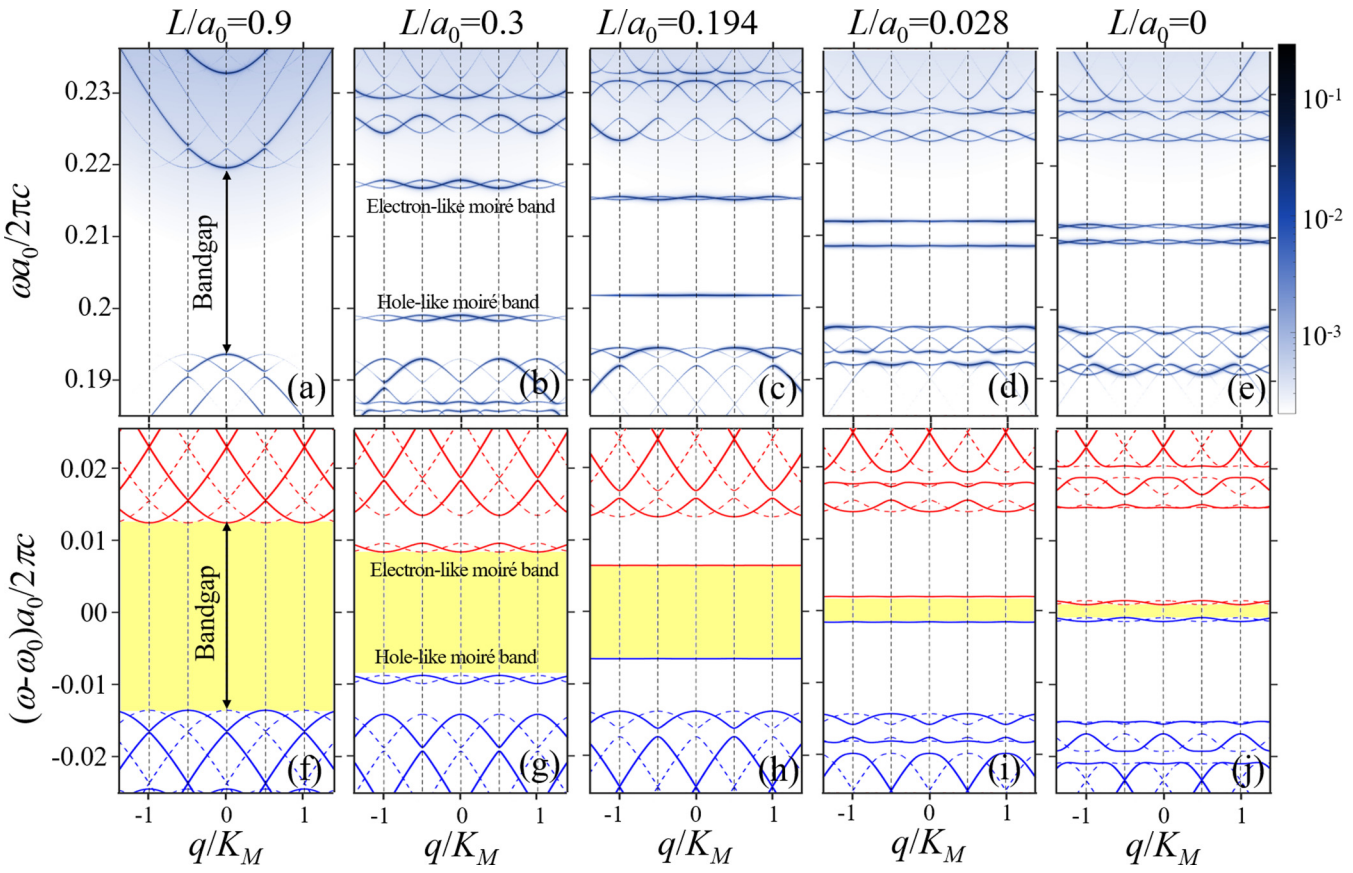

FIG. 2. (a)–(e) Simulated band structures corresponding to different L values. The design for the simulation uses silicon ($n = 3.54$) as the grating material, with $h = 180$ nm, $\kappa = 0.8$, $a_0 = (a_1 + a_2)/2 = 300$ nm, and $N = 13$. The photonic modes of uncoupled gratings are located below the light line, and the interlayer coupling mechanisms, if not strong enough, would not be able to make these modes accessible for rigorous coupled-wave analysis (RCWA) simulations. To solve this, a double-period perturbation of 5% is implemented for the design of each grating. The unit cell in the RCWA simulation consists of two moiré patterns: One is shrunken to 0.95 Λ, and the other one is dilated to 1.05 Λ. (f)–(i) Calculations using the effective Hamiltonian of band structures shown in (a)–(e). To compare with the RCWA simulations having double-period perturbation, dash lines have been added, indicating the folding of the band structure.

global spectral bandwidth of the holelike moiré band of different moiré superlattices ($N = 9$, 13, and 19) when scanning L. These results confirm the existence of magic distances, corresponding to the bandwidth vanishings. All of the analytical calculations are obtained with the same set of parameters that were previously presented. We highlight that the Hamiltonian model provides almost perfectly both the number of magic distances and its values.

For each moiré superlattice (i.e., a given N), our design exhibits two adjustable parameters: (i) the distance L for tuning the interlayer coupling V ($V = V_0$ when $L = 0$ and decreasing exponentially when increasing L [21]) and (ii) the filling fraction κ, defined in Fig. 1, for tuning the intralayer coupling U ($U = 0$ when $\kappa = 1$ and increasing when decreasing κ [21]). Up to now, we have been investigating flatband emergence by scanning L while fixing $\kappa = 0.8$ (i.e., $U = U_0$). However, the direct parameters of the Hamiltonian in Eq. (1) are U, V, and N (from K_M). Thus, a complete picture of magic configuration is captured when varying both V/U (i.e., competition between interlayer vs intralayer coupling) and N (i.e., moiré pattern). Figure 3(d) presents the global bandwidth when scanning N and V/U within a reasonable range [1]. The observed resonant dips correspond to different magic configurations. Dimensional analysis of the Hamiltonian in Eq. (1) suggests that our system is driven by two dimensionless ratios V/U and $U/K_M \sim NU$ [21]. Indeed, fitting the resonances of Fig. 3(d) by a power law, we obtain a very simple empirical relation between the two dimensionless parameters:

$$N_m U = m \times \eta \times \left(\frac{V}{U}\right)^{\gamma}, \qquad m = 1, 2, 3..., \tag{2}$$

with $\gamma \approx -1.42$, $\eta \approx 12U_0$, and m is the *counting order* of the magic configuration. We note that N is the moiré parameter in our system and plays the same role as the *twist angle* in twisted bilayer graphene (each value of the moiré parameter

[1] N is varied from 5 to 30 (If N is too small, the continuum model is not valid. If N is too big, the Brillouin zone becomes too small and bands are naturally very flat). V/U is varied from 0.5 to 2 (If V/U is too small, the approximation $L \ll a_0$ is not valid. If $V/U > 2$, the two moiré bands merge[21])

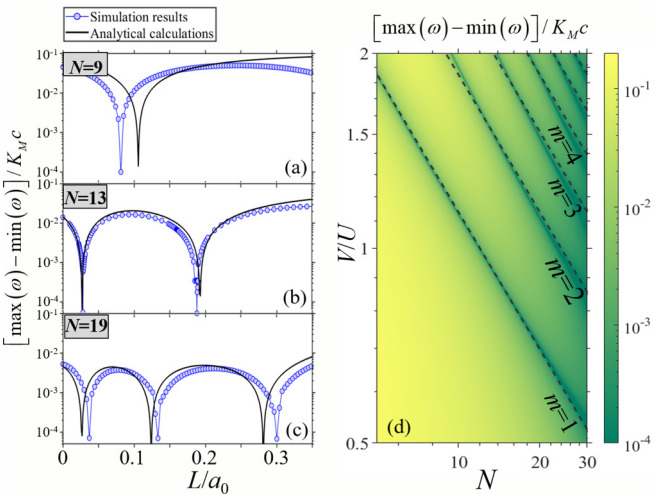

FIG. 3. (a)–(c) The global spectral bandwidth of the holelike moiré band as a function of L for different moiré patterns. Blue circles are results from rigorous coupled-wave analysis (RCWA) simulations. Black lines are analytical calculations. (d) The global spectral bandwidth as a function of V/U and N, with $U = U_0$. The dashed lines correspond to the empirical law in Eq. (2).

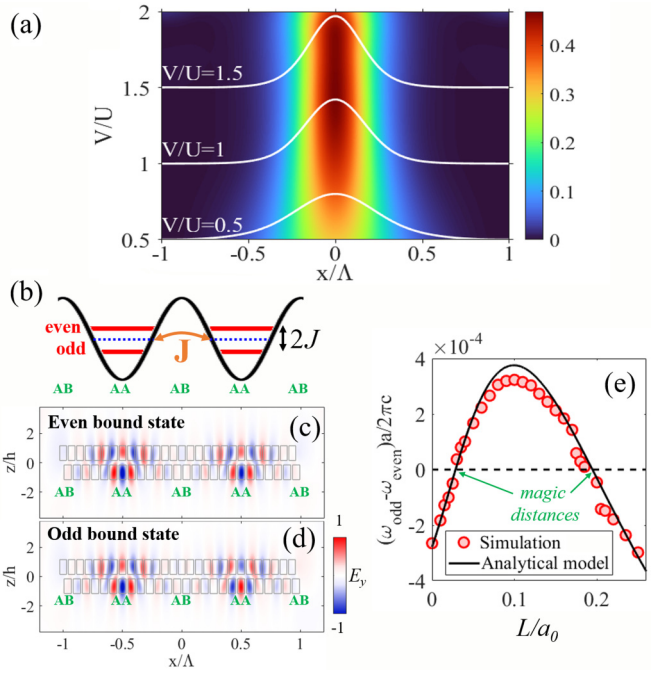

FIG. 4. (a) Wannier function, calculated by the twisted parallel transport gauge [31], of the holelike moiré band when scanning the V/U ratio. (b) Sketch of a holelike diatomic molecule made of two moiré cells. (c) and (d) The field distribution of the two holelike bound states obtained by finite-difference time-domain (FDTD) simulations. The chosen moiré design is the same as the one in the rigorous coupled-wave analysis (RCWA) simulations in Fig. 2. (e) The energy splitting between the two bound states as a function of L. Red circles are results from FDTD simulations, and the solid black line is the result from the effective Hamiltonian. For the analytical calculation, the boundary condition is chosen so that outside of the moiré molecule is a bilayer structure of AB sites, and the bound states are calculated by the transfer matrix method [32,33]. For FDTD simulations, the structure only consists of two moiré cells.

defines a moiré pattern) [26,27]. Therefore, a good metric for magic configurations is the *magic number* N_m, and Eq. (2) provides the design rule to achieve them. The analogy and similitude between this law and the one for magic angles in twisted bilayer graphene [2] are striking, and we expect an appealing interpretation for this simple relation.

Knowing that flatband states would give rise to an unconventional localization regime [12,28,29], we now investigate the localization of light at magic configurations. A closer look at the two moiré bands in Fig. 2 reveals that their dispersion characteristic are nearly single-harmonic functions with the dominance of the first Fourier component with respect to higher orders. Consequently, this suggests that each moiré band may be described by a textbook single-band tight-binding model with only a few nearest neighbor couplings considered. It is of interest to compute the Wannier functions for the band under consideration since they are the natural basis for the tight-binding model [30]. Figure 4(a) depicts the result of this calculation when scanning the ratio V/U, showing that >94% of the Wannier density is located within a single moiré cell. Such a concentration confirms the use of this Wannier function as a pseudo-orbital wave function for the tight-binding model with nearest neighbor couplings. However, it is important to stress that the high concentration of the Wannier function is not necessarily related to flatband formations. However, the physics of the moiré bands can be captured quite well by a simple tight-binding scheme in the Wannier basis. In this scenario, the moiré superlattice engenders a periodic potential landscape with minima at AA sites. Trapped photons in the Wannier states can tunnel to the nearest neighbor ones with tunneling rate J to form moiré bands of bandwidth $2|J|$. As a consequence, when the couple $(NU, V/U)$ satisfies Eq. (2) of magic configurations, the only way to obtain dispersionless bands is that the effective tunneling rate J becomes zero. This leads to the tight localization of light within a single moiré cell at magic configurations. The compact localized states [34] of our localization is simply the Wannier function. We notice a resemblance of the flatband emergence in our system compared with the one in a twisted bilayer graphene system [2,35,36]: both correspond to good localization at the AA sites.

Keeping in mind the ability to localize light to a moiré period with high quality (albeit nonperfect), we investigate a much simpler problem: a diatomic molecule made of two moiré cells [Fig. 4(b)]. Figures 4(c) and 4(d) depict the field distribution of the holelike bound states with even [Fig. 4(c)] and odd [Fig. 4(d)] parity regarding the lateral mirror symmetry. The energy splitting when scanning the distance L is presented in Fig. 4(e). Again, the results from the analytical model and numerical simulations show very good agreement. Notably, these results demonstrate the crossing of these bound states exactly at the magic distances of the moiré superlattice from Fig. 3(b). Consequently, it supports that the tunneling rate J changes sign when scanning L across a magic distance value and vanishes when L takes a magic distance value.

In conclusion, we have investigated theoretically the 1D moiré superlattice of bilayer photonic crystal. All analyti-

cal results derived from a simple effective Hamiltonian are in good agreement with numerical simulations, showing the emergence of flatbands at magic configurations. The conditions for flatbands unify to a nontrivial relation between the counting order of the magic configuration and the magic number, given by $N_m \sim m$. The physics of the moiré minibands is captured by a simple tight-binding model, resulting in localization of photonic states within a single moiré period at flatband configurations when the tunneling rate vanishes accidentally. As a fundamental perspective, the implementation of nonlinearity via Kerr nonlinearity [37] or an exciton-polariton platform [38] would pave the way to investigating the strongly correlated bosonic flatband physics [39–41] with intriguing phases of 1D matters [42]. For applications in optoelectronic devices, the design in this letter uses silicon as a dielectric material, operating in the telecom range with feasible fabrication [25,43,44] and is transferable to 1D integrated optics. The high sensitivity of the dispersion band structure to the refractive index of the surrounding medium (which determines the parameter U) and spacing medium (which determines the parameter V) can be harnessed for applications in sensing. Furthermore, the localization of light within the moiré period also suggests a unique way to engineer the lattice of resonators of a high-quality factor for a phase-locked microlaser array or high Purcell factor for tailoring spontaneous emission of quantum emitters. Another realization scheme is with dual-core fiber Bragg gratings [45,46] to study soliton physics arising from photonic nonlinearity which will be greatly enhanced at flatband configurations [45–47].

The authors thank Stephen Carr, Nguyen Viet Hung, and Steven H. Simon for fruitful discussions. This letter is partly funded by the French National Research Agency under the Project POPEYE (ANR-17-CE24-0020) and the IDEXLYON from Université de Lyon, Scientific Breakthrough Project TORE within the Programme Investissements d'Avenir (ANR-19-IDEX-0005). D.X.N. was supported by Brown Theoretical Physics Center. H.C.N. was supported by the Deutsche Forschungsgemeinschaft (Projects No. 447948357 and No. 440958198), the Sino-German Center for Research Promotion (Project M-0294), and the ERC (Consolidator Grant 683107/TempoQ). RCWA simulations were performed on the CNRS/IN2P3 Computing Center in Lyon.

[1] R. Bistritzer and A. H. MacDonald, Moiré bands in twisted double-layer graphene, Proc. Natl. Acad. Sci. USA **108**, 12233 (2011).

[2] G. Tarnopolsky, A. J. Kruchkov, and A. Vishwanath, Origin of Magic Angles in Twisted Bilayer Graphene, Phys. Rev. Lett. **122**, 106405 (2019).

[3] S. Lisi, X. Lu, T. Benschop, T. A. de Jong, P. Stepanov, J. R. Duran, F. Margot, I. Cucchi, E. Cappelli, A. Hunter, A. Tamai, V. Kandyba, A. Giampietri, A. Barinov, J. Jobst, V. Stalman, M. Leeuwenhoek, K. Watanabe, T. Taniguchi, L. Rademaker *et al.*, Observation of flat bands in twisted bilayer graphene, Nat. Phys. **17**, 189 (2021).

[4] Y. Cao, V. Fatemi, S. Fang, K. Watanabe, T. Taniguchi, E. Kaxiras, and P. Jarillo-Herrero, Unconventional superconductivity in magic-angle graphene superlattices, Nature (London) **556**, 43 (2018).

[5] H. S. Arora, R. Polski, Y. Zhang, A. Thomson, Y. Choi, H. Kim, Z. Lin, I. Z. Wilson, X. Xu, J.-H. Chu, K. Watanabe, T. Taniguchi, J. Alicea, and S. Nadj-Perge, Superconductivity in metallic twisted bilayer graphene stabilized by WSe_2, Nature (London) **583**, 379 (2020).

[6] P. Stepanov, I. Das, X. Lu, A. Fahimniya, K. Watanabe, T. Taniguchi, F. H. L. Koppens, J. Lischner, L. Levitov, and D. K. Efetov, Untying the insulating and superconducting orders in magic-angle graphene, Nature (London) **583**, 375 (2020).

[7] Z. Song, Z. Wang, W. Shi, G. Li, C. Fang, and B. A. Bernevig, All Magic Angles in Twisted Bilayer Graphene are Topological, Phys. Rev. Lett. **123**, 036401 (2019).

[8] S. Wu, Z. Zhang, K. Watanabe, T. Taniguchi, and E. Y. Andrei, Chern insulators, van Hove singularities and topological flat bands in magic-angle twisted bilayer graphene, Nat. Mater. **20**, 488 (2021).

[9] X.-R. Mao, Z.-K. Shao, H.-Y. Luan, S.-L. Wang, and R.-M. Ma, Magic-angle lasers in nanostructured moirésuperlattice, Nat. Nanotechnol. **16**, 1099 (2021).

[10] G. Hu, Q. Ou, G. Si, Y. Wu, J. Wu, Z. Dai, A. Krasnok, Y. Mazor, Q. Zhang, Q. Bao, C. W. Qiu, and A. Alù, Topological polaritons and photonic magic angles in twisted α-MoO_3 bilayers, Nature (London) **582**, 209 (2020).

[11] G. Hu, A. Krasnok, Y. Mazor, C. W. Qiu, and A. Alù, Moiré hyperbolic metasurfaces, Nano Lett. **20**, 3217 (2020).

[12] P. Wang, Y. Zheng, X. Chen, C. Huang, Y. V. Kartashov, L. Torner, V. V. Konotop, and F. Ye, Localization and delocalization of light in photonic moiré lattices, Nature (London) **577**, 42 (2020).

[13] B. Lou, N. Zhao, M. Minkov, C. Guo, M. Orenstein, and S. Fan, Theory for Twisted Bilayer Photonic Crystal Slabs, Phys. Rev. Lett. **126**, 136101 (2021).

[14] K. Dong, T. Zhang, J. Li, Q. Wang, F. Yang, Y. Rho, D. Wang, C. P. Grigoropoulos, J. Wu, and J. Yao, Flat Bands in Magic-Angle Bilayer Photonic Crystals at Small Twists, Phys. Rev. Lett. **126**, 223601 (2021).

[15] K. L. Tsakmakidis, Stopped-light nanolasing in optical magic-angle graphene, Nat. Nanotechnol. **16**, 1048 (2021).

[16] K. L. Tsakmakidis and O. Hess, Extreme control of light in metamaterials: complete and loss-free stopping of light, Phys. B: Condens. Matter **407**, 4066 (2012).

[17] K. L. Tsakmakidis, O. Hess, R. W. Boyd, and X. Zhang, Ultra-slow waves on the nanoscale, Science **358**, eaan5196 (2017).

[18] N is varied from 5 to 30 (if N is too small, the continuum model is not valid. If N is too big, the Brillouin zone becomes too small and bands are naturally very flat). V/U is varied from 0.5 to 2 (if V/U is too small, the approximation $L \ll a_0$ is not valid. If $V/U > 2$, the two moiré bands merge [21]).

[19] A. V. Rozhkov, A. O. Sboychakov, A. L. Rakhmanov, and F. Nori, Electronic properties of graphene-based bilayer systems, Phys. Rep. **648**, 1 (2016).

[20] K. Okamoto, Coupled mode theory, in *Fundamentals of Optical Waveguides*, 2nd ed., edited by K. Okamoto (Academic Press, Burlington, 2006), Chap. 4, pp. 159–207.

[21] See Supplemental Material at http://link.aps.org/supplemental/10.1103/PhysRevResearch.4.L032031 for full derivation details of the Hamiltonian models, the numerical simulations and parameter retrievals from band structure of single layer and bilayer lattices, as well as other further details.

[22] M. G. Moharam and T. K. Gaylord, Rigorous coupled-wave analysis of metallic surface-relief gratings, J. Opt. Soc. Am. A **3**, 1780 (1986).

[23] V. Liu and S. Fan, S4 : A free electromagnetic solver for layered periodic structures, Comput. Phys. Commun. **183**, 2233 (2012).

[24] D. Alonso-Álvarez, T. Wilson, P. Pearce, M. Führer, D. Farrell, and N. Ekins-Daukes, SOLCORE: a multi-scale, Python-based library for modelling solar cells and semiconductor materials, J. Comput. Electron. **17**, 1099 (2018).

[25] H. Nguyen, F. Dubois, T. Deschamps, S. Cueff, A. Pardon, J.-L. Leclercq, C. Seassal, X. Letartre, and P. Viktorovitch, Symmetry Breaking in Photonic Crystals: On-Demand Dispersion from Flatband to Dirac Cones, Phys. Rev. Lett. **120**, 066102 (2018).

[26] J. M. B. Lopes dos Santos, N. M. R. Peres, and A. H. Castro Neto, Graphene Bilayer with a Twist: Electronic Structure, Phys. Rev. Lett. **99**, 256802 (2007).

[27] J. M. B. Lopes dos Santos, N. M. R. Peres, and A. H. Castro Neto, Continuum model of the twisted graphene bilayer, Phys. Rev. B **86**, 155449 (2012).

[28] S. Mukherjee, A. Spracklen, D. Choudhury, N. Goldman, P. Öhberg, E. Andersson, and R. R. Thomson, Observation of a Localized Flat-Band State in a Photonic Lieb Lattice, Phys. Rev. Lett. **114**, 245504 (2015).

[29] R. A. Vicencio, C. Cantillano, L. Morales-Inostroza, B. Real, C. Mejía-Cortés, S. Weimann, A. Szameit, and M. I. Molina, Observation of Localized States in Lieb Photonic Lattices, Phys. Rev. Lett. **114**, 245503 (2015).

[30] N. W. Ashcroft and N. D. Mermin, *Solid State Physics* (Holt, Rinehart and Winston, New York, 1976).

[31] D. Vanderbilt, *Berry Phases in Electronic Structure Theory* (Cambridge University Press, Cambridge, 2018).

[32] J. H. Davies, *The Physics of Low-Dimensional Semiconductors: An Introduction* (Cambridge University Press, Cambridge, 1998).

[33] H. C. Nguyen, M. T. Hoang, and V. L. Nguyen, Quasi-bound states induced by one-dimensional potentials in graphene, Phys. Rev. B **79**, 035411 (2009).

[34] W. Maimaiti, A. Andreanov, H. C. Park, O. Gendelman, and S. Flach, Compact localized states and flat-band generators in one dimension, Phys. Rev. B **95**, 115135 (2017).

[35] A. C. Gadelha, D. A. A. Ohlberg, C. Rabelo, E. G. S. Neto, T. L. Vasconcelos, J. L. Campos, J. S. Lemos, V. Ornelas, D. Miranda, R. Nadas, F. C. Santana, K. Watanabe, T. Taniguchi, B. van Troeye, M. Lamparski, V. Meunier, V.-H. Nguyen, D. Paszko, J.-C. Charlier, L. C. Campos, et al., Localization of lattice dynamics in low-angle twisted bilayer graphene, Nature (London) **590**, 405 (2021).

[36] V. H. Nguyen, D. Paszko, M. Lamparski, B. Van Troeye, V. Meunier, and J.-C. Charlier, Electronic localization in small-angle twisted bilayer graphene, 2D Mater. **8**, 035046 (2021).

[37] D. Rivas and M. I. Molina, Seltrapping in flat band lattices with nonlinear disorder, Sci. Rep. **10**, 5229 (2020).

[38] V. Goblot, B. Rauer, F. Vicentini, A. Le Boité, E. Galopin, A. Lemaître, L. Le Gratiet, A. Harouri, I. Sagnes, S. Ravets, C. Ciuti, A. Amo, and J. Bloch, Nonlinear Polariton Fluids in a Flatband Reveal Discrete Gap Solitons, Phys. Rev. Lett. **123**, 113901 (2019).

[39] D. Leykam, J. D. Bodyfelt, A. S. Desyatnikov, and S. Flach, Localization of weakly disordered flat band states, Eur. Phys. J. B **90**, 1 (2017).

[40] C. Danieli, A. Andreanov, and S. Flach, Many-body flatband localization, Phys. Rev. B **102**, 041116(R) (2020).

[41] E. Khalaf, S. Chatterjee, N. Bultinck, M. P. Zaletel, and A. Vishwanath, Charged skyrmions and topological origin of superconductivity in magic angle graphene, Sci. Adv. **7**, abf5299 (2021).

[42] T. Giamarchi, *Quantum Physics in One Dimension* (Oxford University Press, Oxford, 2003).

[43] Y. Shuai, D. Zhao, Y. Liu, C. Stambaugh, J. Lawall, and W. Zhou, Coupled bilayer photonic crystal slab electro-optic spatial light modulators, IEEE Photon. J. **9**, 1 (2017).

[44] S. Cueff, F. Dubois, M. S. R. Huang, D. Li, R. Zia, X. Letartre, P. Viktorovitch, and H. S. Nguyen, Tailoring the local density of optical states and directionality of light emission by symmetry breaking, IEEE J. Sel. Top. Quantum Electron. **25**, 1 (2019).

[45] W. C. K. Mak, P. L. Chu, and B. A. Malomed, Solitary waves in coupled nonlinear waveguides with Bragg gratings, J. Opt. Soc. Am. B **15**, 1685 (1998).

[46] T. Ahmed and J. Atai, Soliton-soliton dynamics in a dual-core system with separated nonlinearity and nonuniform Bragg grating, Nonlinear Dyn. **97**, 1515 (2019).

[47] B. J. Eggleton, R. E. Slusher, C. M. de Sterke, P. A. Krug, and J. E. Sipe, Bragg Grating Solitons, Phys. Rev. Lett. **76**, 1627 (1996).